Spring 5-1-2009

# The Synthesis and Characterization of Novel Microporous Hybrid Organic/Inorganic Materials

Kelly Whitenack

# SECTION I:

# INTRODUCTION, EXPERIMENTAL BACKGROUND AND THEORY

## 1.1 INTRODUCTION

In the past two hundred years, the world population has increased dramatically. To put the population growth curve into perspective: It took all of human history until about 1830 to reach the first billion.[4] The next billion took 100 years (1930); the third billion, 30 years (1960); the fourth billion, 15 years (1975); the fifth billion, 12 years (1987); the sixth billion, 12 years (1999); and with the current slowing trend, the next billion will take about 14 years.[4] An unknown writer claims that three-quarters of all the people who have ever been born are alive today. With the dramatic increase in the world population the past two centuries, industrial development has soared. One of the products of the rise in industrial development is the automobile. It was 1885 when Karl Benz built the first automobile powered by an internal-combustion engine and 28 years later Henry Ford first mass produced the automobile in 1913.[5] Industrial development has come a long way from the days of Benz and Ford, as has the knowledge of the environmental repercussions of the internal-combustion engine.

Today our world's fleet of automobiles smothers communities in pollution and contributes 25 percent of the emissions that cause climate change through global warming.[6] Global warming has been a recent political debate, and its main focus is the emission of greenhouse gases. The

greenhouse effect occurs when harmful gases accumulate in the atmosphere and act like the glass roof of a greenhouse, trapping the heat radiating from the earth's surface when the sun's radiation hits.[4] Greenhouse gases, which include $CO_x$, $NO_x$, $SO_x$, $CH_4$, and hydrocarbons (all products of diverse human activities), are solely responsible for manmade contributions to global warming. "Under business as usual, we'll reach carbon dioxide concentrations that haven't been seen on this planet in the past 50 million years," Harvard professor and Nobel Laureate John Holdren told a recent White House conference on global warming. "We will have achieved that in the geological blink of an eye, exposing, as we do it, natural systems to a rate of temperature change faster than at any time in the last 10,000 years."[7]

With this in mind, scientists have been trying to develop novel materials to aid in the decrease of greenhouse gasses. A new idea for an alternative to fossil fuel has been hydrogen gas since it adds fewer pollutants into the environment. There are several limitations to the idea of using hydrogen gas as a fossil fuel alternative, with the most obvious being gas storage. Keeping the Hindenburg disaster in mind, would you want to have a hydrogen tank strapped to your car?

A Metal Organic Framework (MOF) is an organic-inorganic hybrid material in which metal atoms or clusters are bridges by polyfunctional organic molecules.[3] MOF materials have a wide range of physical properties and application, which is one idea driving the investigation into the discovery or new and useful hybrid materials for gas storage. MOFs encompassing

microporosity character are characteristic of large surface areas and permanent porosity and have recently appeared in the limelight due to their potential as hydrogen storage materials for mobile applications.[8] Microporocity, gas storage, and magnetism are a few physical properties of MOFs this research will focus. Due to the most recent energy crisis, the scope of this research will focus on synthesizing an MOF with impressive gas storage and accumulation properties.

Hydrogen acts not an energy source, but an energy carrier. Hydrogen is the new sought after energy carrier, since its application as a fuel creates neither air pollution nor greenhouse gases.[8] Hydrogen storage systems are in high demand due to important environmental and energy repercussions [9,10] and The United States Department of Energy has recognized the need for hydrogen storage systems by setting energy density goals for microporous materials. By 2010 the U.S. Department of Energy has set and energy density goal for hydrogen storage of 6.0% (45kg $H_2$ per $m^3$) by weight and 9.0% (81kg $H_2$ per $m^3$) by 2015.[9,10] These conditions are extremely difficult to achieve considering 5.0kg of hydrogen gas occupies a volume of 56$m^3$ under ambient conditions. Inorganic chemistry is not only essential to the formulation and improvement of modern materials, but also has a huge impact on environmental and biological applications.[1]

New materials must be synthesized which can store large amounts of hydrogen at high temperatures and low pressures, with small volume and low weight, to power future $H_2$-powered vehicles.[8] Contribution to the design and

development of MOFs require hydrothermal synthesis, or high temperatures in which the structural elements of the organic compounds are retained. Hydrothermal synthesis and the advancing MOFs on which this investigation focuses may provide a molecule, which may contribute to $H_2$-powerd vehicles and $H_2$ storage systems.

## 1.2 Properties of Hybrid Organic-Inorganic Materials

### 1.2.1 Microporocity

Currently, there are no practical means of storing hydrogen for transportation.[8] Although there are currently Hydrogen fuel cells for cars, a pure platinum electrode is required, which is quite costly and difficult to mass-produce. Microporous materials may provide a means for both storing and transporting hydrogen gas depending on the size, shape and physical properties of the material's pore.

Porous materials may be characterized from pore size, pore surface area, and/or their adsorption properties. Porous materials are classified on the basis of gas adsorption properties and International Union of Pure and Applied Chemistry (IUPAC) classifications have been established for the classification of pore sizes. The IUPAC classification standards reflect the relationship between porosity and sorption of the molecule (**Table 1.1**).[11]

**Table 1.1** IUPAC Classification of Pores.[11]

| Pore type | Pore size [Å] |
|---|---|
| Ultramicropore | <5 |
| Micropore | 5–20 |
| Mesopore | 20–500 |
| Macropore | >500 |

The IUPAC classifications of pore sizes only describe the size, not the shape of the pore. The MOFs of this research encompass a pore width of 5-20Å, classifying the materials as microporous.

In microporous materials, gases interact with the organic walls of the pores via Van Der Waals forces. Much weaker than chemical bonds, Van Der Waals forces (dispersion forces) are weak intermolecular attractive forces between molecules.[12] These forces allow the hydrogen or nitrogen gas to store within the organic pores of the compound. The desired application of gas storage in MOFs is directly proportional to the diameter; therefore, the pore size and shape is of importance in synthetic schemes. The pore size and shape are determined both by both the metal and the organic ligands incorporated in the synthesis. By using various organic ligands and metals, microporous materials may be assembled using varying synthetic procedures to the chemist's desired size and shape. Various ligands and metals are used in this investigation to construct novel organic-inorganic materials that are microporous.

### 1.2.2 **Gas Storage**

The porosity of MOFs is determined from their ability, or lack thereof, to have a nitrogen or hydrogen gas uptake. When determining gas storage characteristics, nitrogen gas is the most commonly used adsorbate because $N_2$ has permanent quadrupole moment, the level of specificity on most surfaces is not too strong for $N_2$, and liquid and gaseous $N_2$ are readily available and inexpensive.

Historically speaking, porous materials are defined in terms of their adsorption properties.[13] To determine if a compound is actually a microporous material, adsorption isotherms are experimentally determined. IUPAC conventions have been proposed for classifying pore sizes and gas sorption by isotherms that reflect the relationship between porosity and adsorption.[14] The IUPAC classification standards of adsorption isotherms are illustrated in **Figure 1.1**. [11]

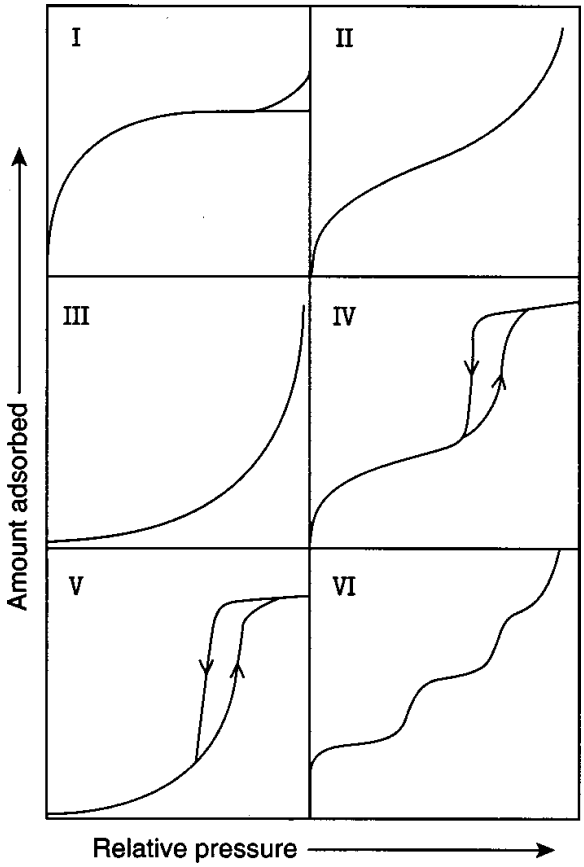


**Figure 1.1 Adsorption isotherm IUPAC classification.**[15]

For physical adsorption (sometimes referred to as van der Waals adsorption), five distinct types of isotherms have been observed.[16] Experimentally obtaining an adsorption isotherm demonstrating Type I absorption as seen in **Figure 1.1** classifies the compound as Type I microporous. It is seen that microporous isotherms (type I) are less than 2 nm in diameter; macroporous isotherms (type II, III, and VI) are greater than 50 nm in diameter; and mesoporous isotherms (type IV and V) are between 2 and 50 nm is diameter.[11,15] A Type I isotherm indicates the sample contains micropores and only micropores and is observed in materials such as charcoal, silica, molecular sieves, stannic oxide gel and ammonium

phosphomolybdate.[17] In Type I isotherms, inaccuracies may occur because of activated passage of molecules through fine restrictions and also pore filling because potential fields from opposite walls overlap, increasing attractive force on adsorbate molecules as compared to larger pores.

The difference between type II and III isotherms and between types IV and V isotherms is due to the relative strengths of the fluid-solid interactions; where as types III and V are associated with weaker fluid-solid molecular interactions.[14]

An equation that relates the amount of a substance attached to a surface to its concentration in the gas phase or in solution, at a fixed temperature, is known as an adsorption isotherm.[18] The concept of adsorption as related to an area of exposed surface was developed by Irving Langmuir[19] in his work on the "condensation" of gases on surfaces. From these studies emerged the concept of adsorption as a dynamic equilibrium between a gas and a solid surface resulting in a surface layer that is only one layer thick. These adsorption concepts led to the BET treatment of multilayer adsorption.[20]

If an MOF possesses the ability to uptake $N_2$ or $H_2$, a series of manipulations are carried out and an adsorption isotherm equation is implemented to find the total surface area of the molecule. The adsorption isotherm used for this purpose is the BET isotherm. The BET isotherm equation was proposed in 1938 by American scientists Stephen Brunauer (1903-1986), Paul Emmett (1900-1985) and Edward Teller (b. 1908) and is

particularly useful for estimating surface areas of porous structures.[18] The behavior of adsorbed molecules is even more difficult to describe in detail than that of molecules in the liquid state; therefore, the BET theory contains some drastic assumptions.[16] However, it is still a generally useful theory of physical gas adsorption. A BET isotherm is not accurate at all pressures, but it is widely used in industry to estimate the surface area of solid materials.[21] Illustrated below in **Eq.** (**1**), The B.E.T. equation traditionally reads

$$\frac{1}{Q\left(\frac{P}{P_0}-1\right)} = \frac{C-1}{V_m C}\left(\frac{P}{P_0}\right) + \left(\frac{1}{V_m C}\right) \qquad (\mathbf{1})$$

Where Q is the absorbed quantity of gas, $\left(\frac{P}{P_0}\right)$ is the ratio of equilibrium and saturation pressure of absorbates; C is the B.E.T. constant found by $C = \frac{S_{slope} + Y_{INT}}{Y_{INT}}$, and $V_m$ is the volume of the monolayer, which is determined by $V_m = \frac{1}{C \times Y_{INT}} = \frac{1}{S_{Slope} + Y_{INT}}$. Eq. (1) has a linear relationship, where in the format of $y = mx + b$, $m$ (the slope) is equivalent to $\left(\frac{C-1}{V_m C}\right)$ and $b$ (the Y intercept) is equivalent to $\left(\frac{1}{V_m C}\right)$.[18] The B.E.T. constant C is large when the enthalpy of desorption from a monolayer is large compared with the enthalpy of vaporization of the liquid adsorbate[21]:

$$C = e^{(\Delta_{des} H^{\phi} - \Delta_{vap} H^{\phi})/RT} \qquad (2)$$

The volume adsorbed (in $cm^3$ at standard pressure and temperature: p = 1 atm, T = 273.15 K) is related to *n*, the number of moles adsorbed, by

$$\upsilon = nRT_0 \tag{3}$$

where $T_0$ = 273.15 K and R = 82.06 $cm^3$ atm.[16] The total area of the solid is given by

$$A = N_0 n_m \sigma \tag{4}$$

where $N_0$ is Avagadro's number (6.022142 $\times$ $10^{23}$ $mol^{-1}$) and $\sigma$ is the cross-sectional area of an adsorbed molecule.[16] The BET equation provides a means to determine the total surface area of a MOF, which helps prove porosity. The total surface area is determined by Eq. (5) below

$$S_{total} = \frac{V_m N s}{V} \tag{5}$$

where V is the molar volume of the adsorbent gas and s is the adsorption cross section. From Eq. (5), the specific surface are may be calculated using

$$S = \frac{S_{total}}{a} \tag{6}$$

where $S_{total}$ is determined using Eq. (5) and a is the weight of the sample in its solid state.

The BET equation is based on a physical model. The important assumptions of the physical model are as follows:[16] 1) The surface of the solid adsorbant is uniform, 2) adsorbed molecules in the first layer are localized, 3) each adsorbed molecule in the first layer provides a site for adsorption of a gas molecule in a second layer, 4) there is no interaction between molecules in a given layer and 5) all molecules in the second and higher layers are assumed

to be like those in the bulk liquid and in particular, the energy of those molecules is taken to be the same as the energy of a molecule in the liquid.[16]

When obtaining an adsorption isotherm $N_2$ or $H_2$ is used. Since such adsorption is caused by forces very similar to those that cause the condensation of a gas to a bulk liquids, appreciable adsorption occurs only at temperatures near the boiling point of the adsorbate.[16] For example, the adsorption of $N_2$ gas on a high-area solid is studied at 77.4 K, the boiling point of liquid nitrogen.

### 1.2.3 **Magnetism**

Magnetic storage and biomedicine are two fields in which the use of magnetic materials is applied. In biomedicine, magnetic cell sorting and magnetic fluid hypothermia are two areas of emerging interest in the application of magnetic materials.[22]

When classifying magnetic materials, compounds may either be diamagnetic or paramagnetic where they are repelled by a magnetic field and attracted by a magnetic field, respectively.[1] Specifically in the inorganic-organic materials on which this research focuses, ferromagnetism, ferrimagnetism and antiferromagnatism are areas of interest when considering magnetic properties. In a ferromagnetic substance the spins on different metal centres are couples into a parallel alignment that is sustained over thousands of atoms in a magnetic domain.[1] In an antiferromagnetic substance, neighboring spins are locked into an antiparallel alignment and the sample has

a low magnetic moment.[1] The third type of collective magnetic interaction is ferrimagnetism. In ferrimagnetism, net magnetic ordering is observed below the Curie temperature ($T_c$); however, ferrimagnets differ from ferromagnetic because ions with different local moments are present.[1]

The triazolate ligand class used in this research has the ability to bridge multiple metal sites, and a superexchange capacity may reflect in unusual magnetic properties. With respect to multifunctionality, magnetism is an important characteristic because an attractive goal is to design a microporous material that is also a magnetic material.

Magnetic measurements of a complex may be used to determined the number of unpaired spins in a complex and hence to identify its ground-state configuration.[1] When considering magnetic properties, crystal field theory cannot be ignored.

Crystal-field theory concentrates on the resulting splitting of the *d* orbitals into groups with different energies and uses that splitting to rationalize and correlate the optical spectra, thermodynamic stability, and magnetic properties of complexes.[1] Depending on the ligand coordinated to a medal, the *d* orbitals can display weak crystal field splitting or strong crystal field splitting. Ligands are either weak field ligands or strong field ligands based on the spectrochemical series. Ryutaro Tsuchia proposed that ligands could be arranged in a spectrochemical series in which the members are arranged in order of increasing energy of transitions that occur when they are present in a complex (**Figure 1.2**).[1]

$I^- < Br^- < S^{2-} < SCN^- < Cl^- < NO^{3-} < F^- < OH^- < C_2O_4^{2-} < H_2O < NCS^-$

$< CH_3CN < NH_3 <$ en $<$ bipy $<$ phen $< NO^{2-} < PPh_3 < CN^- < CO$

**Figure 1.2:** Spectrochemical Series[1]

In the presence of a weak field ligand the valence electrons occupy the eg orbital before doubly occupying the $T_{2g}$ orbital. In the presence of a strong field ligand, the valence electrons fill $T_{2g}$ orbital before occupying the eg orbital. In the presence of weak field ligands, there are a higher number of un-paired electrons resulting in a high spin state. Understanding the various ligands in the spectrochemical series of crystal field theory is important when considering characteristics like magnetism.

However, in the presence of strong field ligands, there are fewer un-paired electrons, resulting in a low spin state. Depending on external conditions (temperature, pressure, electromagnetic radiation, etc.) a low spin to high spin interconversion may occur in a system, altering the compound's magnetic properties. **Figure 1.3** illustrates this phenomena for a Fe(II) $3d^6$ system.

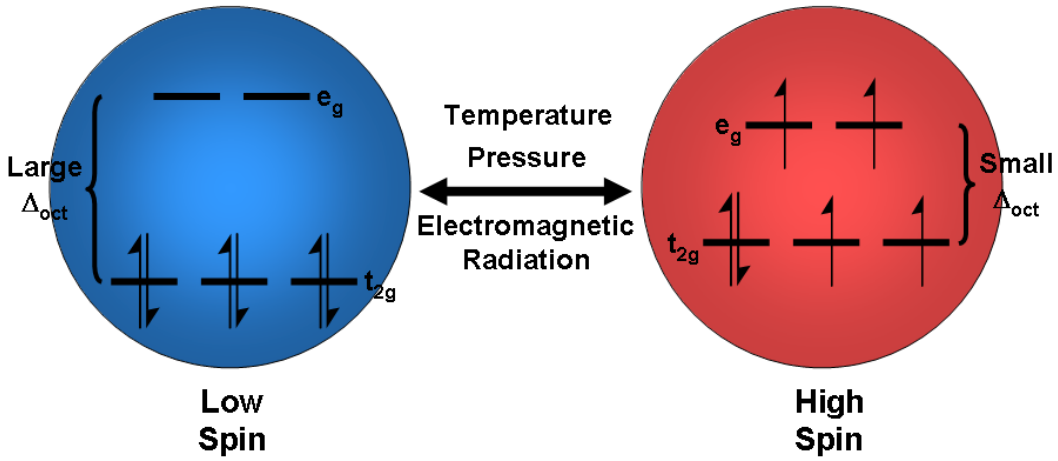


**Figure 1.3** Low Spin to high Spin interconversion for a Fe (II) $3d^6$ system[8]

Materials which exhibit magnetic properties typically contain an octahedral-coordinated transition metal ion with the $3d^n$ ($4 \leq n \leq 7$) electronic configuration and show a spin-crossover between low-spin (LS) and high-spin (HS) state.[23] Low-spin to high-spin conversions may be altered using differing temperatures and pressures. This is noteworthy because the MOFs in this research are synthesized using varying temperatures and at high pressures. In this research, numerous organic ligands lying in different areas of the spectrochemical series are used for ligation; therefore, the magnetic character of each compound will vary.

## 1.3 Hybrid Organic-Inorganic Materials

There are various properties offered by both organic and inorganic molecules. This research involves creating a multifunctional compound incorporating the two species. The design of organic-inorganic hybrid materials conceives of the metal, metal cluster, or metal oxide substructure as

a node from which rigid or flexible multitopic organic ligands radiate to act as tethers to adjacent odes in the bottom-up construction of complex extended architectures (**Figure 1.4**).[3]

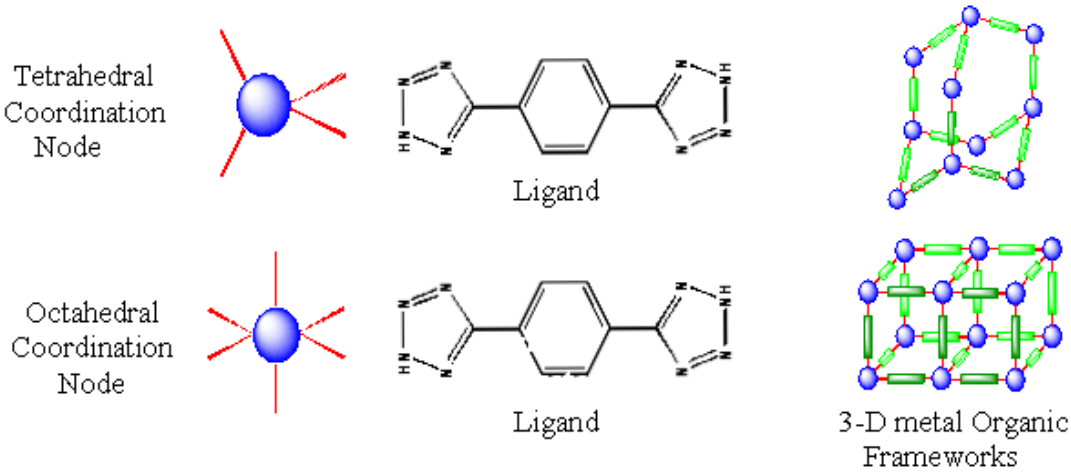


**Figure 1.4** Metal organic framework model

The organic ligands vary in size and shape, and may be rigid or flexible. Simple ligand modifications are usually reflected in the properties of the materials. The varying properties of the metal nodes and organic ligands contribute to the varying physical properties of the metal organic frameworks synthesized.

Two categories of such materials have been identified: metal organic frameworks and metal oxide hybrids in which metal-oxygen-metal arrays are embedded within the architectures [24,25]; however, the scope of this research will focus on just metal organic frameworks.

## 1.4 Organic Ligands

### 1.4.1 Representative Ligands/Properties

A ligand is an ion or molecule that may have an independent existence[1] and it usually surrounds metal ions to form complexes. An example of a complex is $[Co(NH_3)_6]^{3+}$ where the metal cobalt$^{3+}$ is surrounded by six $NH_3$ ligands. In this example, the $NH_3$ molecule is a ligand because it may exist independently from the Co (III) ion. There are thousands of different ligands; therefore, there are many different categories in which they are organized. One way to classify ligands is the number of attachment points they have with the metal. Ligands that have only one point of attachment to the metal are called monodentate ligands while ligands that have more than one point of attachment are classified as polydentate ligands. Ligands that specifically have two points of attachments are known as bidentate; those with three, tridentate, and so on.[1] Multidentate ligands whose stereochemistry allows two or more donor atoms to be simultaneously bonded to the same metal are often observed.[26] These complexes are also known as chelates. When a chelate is formed, the potential of having a porous material is more likely. In addition, the metal complexes formed by chelating ligands are nearly always more stable than those formed by their monodentate analogues (the chelate effect) and this is illustrated quantitatively by the thermodynamic data obtained from the interaction of metal ions with the bidentate ligand 1,2-diaminoethane (en) and with the monodentate one, methyamine.[26] Multidentate ligands will be mainly used in this research because of this

characteristic. A metal organic complex that is both porous and thermodynamically stable is ideal for the investigation of hydrogen storage systems.

One of the most general ways to describe the bonding of a ligand to a metal is a topic learned in general chemistry: acids and bases. The Lewis definitions of acids and bases provide for a general view as to why ligands have donor atom characteristics. A Lewis acid is an electric-pair acceptor while a Lewis base is an electron-pair donor.[27] Therefore, the ligand that donates electrons to bond to a metal is acting as a Lewis base, while the metal a Lewis acid. For the example of $[Co(NH_3)_6]^{3+}$, $NH_3$ acts as a Lewis base, donating its electron pair to Co(III).

### 1.4.2 Polyazoheteroaromatic Compounds

The most recent attention when considering organic ligands in MOFs has focused on Polyazaheteroaromatic ligands[28] and these compounds are a classification of ligands used in this research. Polyazoheteroaromatic compounds, also known as trizolates, are five membered aeromatic compounds containing at least one nitrogen atom. Polyazoheteroaromatics are a class of ligands that has been the main focus of many recent studies due to their technological application and widespread use as a bridging ligand.[3] A few of the more common Polyazoheteroaromatic compounds include pyrazole, imidazole, triazole and tetrazole (**Figure 1.5**).[29]

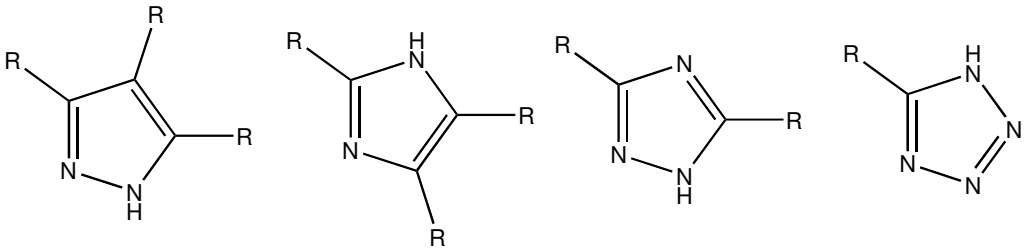


**Figure 1.5** Neutral Polyazoheteroaromatic Organic Ligands [29]

In their neutral and anionic forms, these compounds are exploited in the construction of complex organic-inorganic architectures.[29] Coordination compounds of 1,2,4-triazoles exhibit unusual structural diversity as a result of the di- and trinucleating properties of the neutral and anionic ligand forms, respectively.[3] In addition, polyazaheteroaromatic ligands have been shown to bridge metal ions to afford polynuclear compounds, to possess superexchange capacity resulting in unusual magnetic properties of the complexes and to be readily derivatized to incorporate additional functional and/or steric groups.[30]

Polyazoheteroaromatic ligands are attractive in the synthesis of metal organic frameworks due to their ability to bridge multiple metal sites through their N1 and N2 positions.[29] These structural building blocks are what this research is based on, and the MOFs synthesized may provide the most novel microporous structure. Taking advantage of the structural diversity an organic ligand may possess, six organic tethers based on Polyazoheteroaromatic compounds are synthesized to combine with metal nodes with the objective of creating an ideal microporous metal organic framework.

### 1.4.3 Benzyl Tetrazole

The first ligand synthesized is benzyl tetrazole. Triethylamine chlroide, sodium azide, and benzonitrile in a mole ratio of 2:2:1 was added to 150 mL toluene and 30 mL methanol. This solution was allowed to reflux at 80$^{o}$C for 72 hours and was followed by a 100 mL NaOH workup. The organic layer was obtained by use of a sepratory funnel and the precipitate was obtained by adding HCl dropwise (about 20 drops). Using this synthetic scheme, benzyl tetrazole (**Figure 1.6**) was obtained in 66.6 % yield.

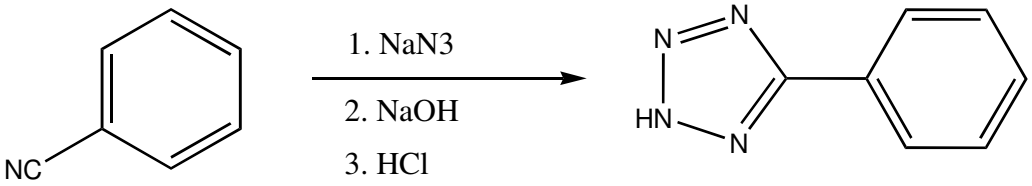


**Figure 1.6** Benzyl Tetrazole Synthesis

The benzyl tetrazole ligand is a tridentate ligand, with three potential nitrogen lone-pair donors. Benzyl tetrazole has the ability to bridge multiple metal sites through their N1, N3 and N4 positions.

### 1.4.4 2-Pyridine Tetrazole

Triethylamine chlroide, sodium azide and 2-cyanopyridine in a mole ratio of 2:2:1 was added to 150 mL toluene and 30 mL methanol. This solution was allowed to reflux at 80$^{o}$C for 72 hours and was followed by a 100 mL NaOH workup. The organic layer was obtained by use of a sepratory funnel and the precipitate was obtained by adding HCl dropwise (about 20

drops). Using this synthetic scheme, 2-pyridine tetrazole (**Figure 1.7**) was obtained in 41.3 % yield.

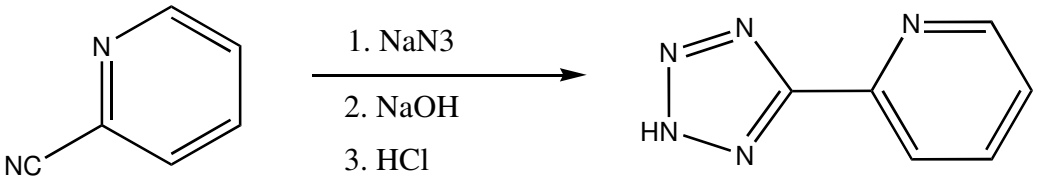


**Figure 1.7** 2-Pyridine Tetrazole Synthesis

The 2-pyridine tetrazole ligand is a multidentate ligand, with four potential nitrogen lone-pair donors.

### 1.4.5 Pyrazine Tetrazole

Triethylamine chlroide, sodium azide and pyrazine carbonitrile in a mole ratio of 2:2:1 was added to 150 mL toluene and 30 mL methanol. This solution was allowed to reflux at 80$^{o}$C for 72 hours and was followed by a 100 mL NaOH workup. The organic layer was obtained by use of a sepratory funnel and the precipitate was obtained by adding HCl dropwise. Using this synthetic scheme, 2-pyridine tetrazole (**Figure 1.8**) was obtained in 72.3 % yield.

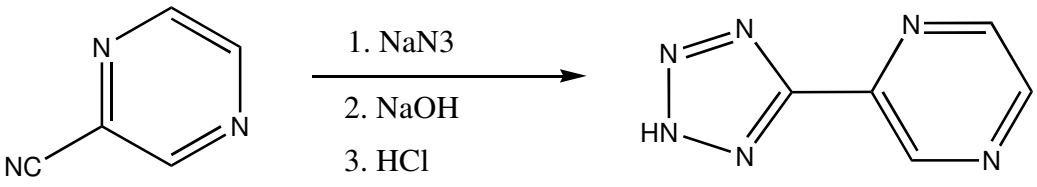


**Figure 1.8** Pyrazine Tetrazole Synthesis

The pyrazine tetrazole ligand is a multidentate ligand, with five potential nitrogen lone-pair donors.

### 1.4.6 3-Tetrazole Benzoic Acid

Triethylamine chlroide, sodium azide and 3-cyano benzoic acid in a mole ratio of 2:2:1 was added to 150 mL toluene and 30 mL methanol. This solution was allowed to reflux at 80$^{o}$C for 72 hours and was followed by a 100 mL NaOH workup. The organic layer was obtained by use of a sepratory funnel and the precipitate was obtained by adding HCl dropwise. Using this synthetic scheme, 2-pyridine tetrazole (**Figure 1.9**) was obtained in 62.09 % yield.

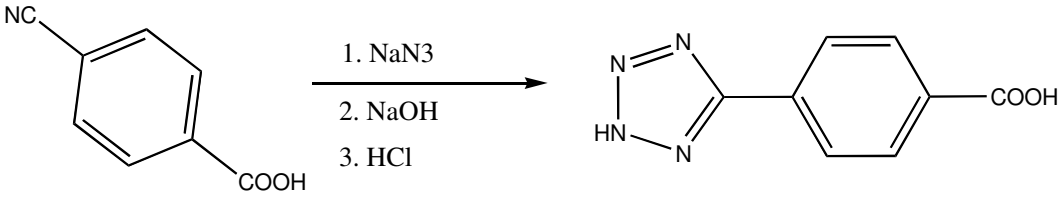


**Figure 1.9** 3-Tetrazole Benzoic Acid Synthesis

The 3-tetrazole benzoic acid ligand is a tridentate ligand, with three potential nitrogen lone-pair donors.

### 1.4.7 4-Tetrazole Benzoic Acid

Triethylamine chlroide, sodium azide and 4-cyano benzoic acid in a mole ratio of 2:2:1 was added to 150 mL toluene and 30 mL methanol. This

solution was allowed to reflux at 80°C for 72 hours and was followed by a 100 mL NaOH workup. The organic layer was obtained by use of a sepratory funnel and the precipitate was obtained by adding HCl dropwise. Using this synthetic scheme, 2-pyridine tetrazole (**Figure 1.10**) was obtained in 79.59 % yield.

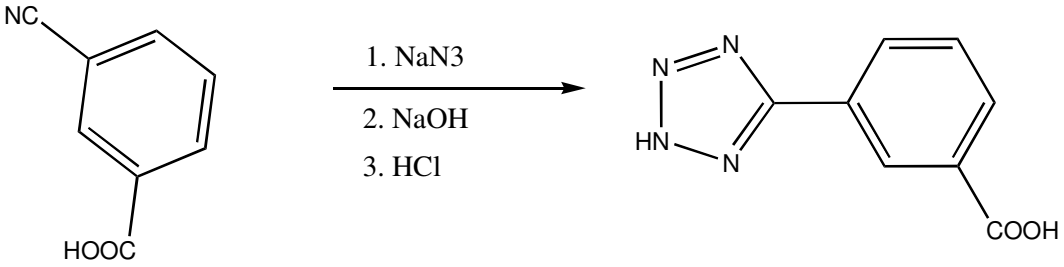


**Figure 1.10** 4-Tetrazole Benzoic Acid Synthesis

The 4-tetrazole benzoic acid ligand is a multidentate ligand, with three potential nitrogen lone-pair donors and a carboxylic acid. The two ligands 4-tetrazole benzoic acid and 3-tetrazole benzoic acid are very similar, differing in the position of the carboxylic acid. Varying the position of the carboxylic acid, may allow for the variation in pore size and shape, leading to various gas uptake properties.

### 1.4.8. 1,4-Benzene Ditetrazole Synthesis

The precurser 1,4-Dicyanobenzene is obtained through the cyanation reaction of 1,4-Dibromobenzene, CuCN and DMF. This solution was refluxed at 130°C for 72 hours. Triethylamine chloride, sodium azide, and 1,4-Dicyanobenzene in a mole ratio of 2:2:1 was added to 150 mL toluene and 30 mL methanol. This solution was allowed to reflux at 80°C for 72 hours and

was followed by a 100 mL NaOH workup. The organic layer was obtained by use of a sepratory funnel and the precipitate was obtained by adding HCl dropwise. Using this synthetic scheme, 1,4-benzene ditetrazole (BDT) (**Figure 1.11**) was obtained in 89.0% yield.

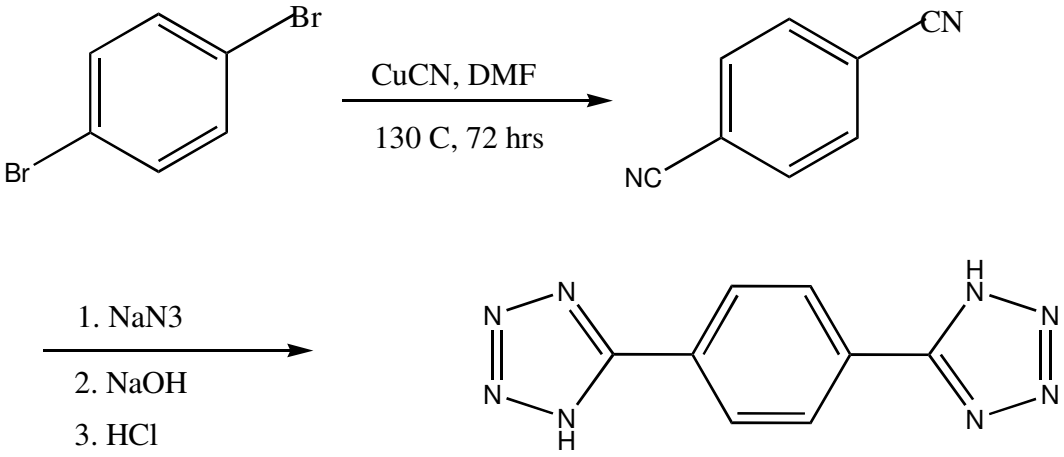


**Figure 1.11** 1,4-Benzene Ditatrazole Synthesis [131,32,33]

The BDT ligand is a multidentate ligand, with six potential nitrogen lone-pair donors. Similar ligands are pyridine and its chelating analogues bipyridyl (bipy) and phenanthroline (phen).

One general feature of organic ligands is that with metal cations having a co-ordination number twice as large as the oxidation number, they form neutral complexes that are appreciably soluble in organic solvents.[26] This is a noteworthy feature because soluble complexes are needed when synthesizing a material hydrothermally.

## 1.5 Hydrothermal Synthesis

Contributions to the design and development of microporous materials require the application of hydrothermal synthesis due to this method's ability to allow the composition of metal organic compounds to be controlled. The synthesis of metal organic compounds requires high temperatures in which the structural elements of the organic compounds are retained while both the organic and inorganic compounds are solubilized.

**Figure 1.12** Teflon-lined Parr bombs used for hydrothermal synthesis

Hydrothermal synthesis also stabilizes low temperature phases and materials with elements containing unusual oxidizing states.

Hydrotheramal synthesis is carried out in 25 mLTeflon lined, stainless steel Parr Bombs (**Figure 1.14**) which have the ability to withstand high temperatures and pressures. Hydrothermal synthesis is one of the most successful methods in preparing metal organic crystals for the scope of this research.

## 1.7 Physical Techniques in Inorganic Chemistry

### 1.7.1 Diffraction Methods

X-ray diffraction is by far the greatest source of information on crystal and molecular structures and at high precision can reveal fine details of the electron density distribution of a molecular structure.[34] It was 1912 when the German physicist Max von Laue reasoned that if crystals did consist of a regular array of atoms, then a crystal should act as a three-dimensional grating capable of diffracting short wavelength radiation such as X-rays.[35]

One of the most powerful applications of X-ray diffraction is crystal structure determination and refinement, which is carried out using the intensities of thousands of reflections collected from a single crystal.[35] The method allows for the unambiguous determination of the positions of the atoms and ions that make up a molecular or ionic compound, allowing description of structures in terms of features such as bond lengths and angles and the relative positions of ions and molecules in a unit cell.[1] X-ray diffraction has been responsible for determining the structures of a quarter of a million different substances, including tens of thousands of purely inorganic compounds and many more organometallic compounds[1]. X-ray diffraction is the technique responsible for determining the structures of the materials synthesized in this research.

There are two principal X-ray techniques: the powder method and single-crystal diffraction. In the powder method, the materials being studied are in polycrystalline form, consisting of thousands of crystallites of a few

micrometers or less in dimension.[1] In single-crystal diffraction, the compound is available as a single crystal of dimensions of several tens of micrometers or larger. Some of the many applications of X-ray diffraction include identification of unknown materials, determination of a sample's purity, determination and refinement of lattice parameters, investigation of phase diagrams and new materials, determination of crystallite size and stress, structure refinement and phase changes. This research will employ the single-crystal method, where larger crystals are needed for diffraction.

### 1.7.2 Thermal Gravimetric Analysis

Thermal gravimetric analysis (TGA) is a technique examining the weight loss of a material as a function of temperature. This allows the physical properties of porous materials and stability to be determined. This analysis is represented as a plot of mass percent versus temperature, to allow the weight loss (water, solvents, etc.) to be examined. As the temperature increases, these systems can lose weight from the chemical reaction liberating gas. The system can also lose weight from the breaking down of the actual framework, and this feature gives chemists insight into the material's stability characteristics. This is an imperative principal of thermal analysis when studying solid state and material chemistry and will be a physical application used heavily throughout this research.

### 1.7.3 Infrared Resonance Spectroscopy

The interactions of electromagnetic radiation with matter serve as one of the most useful methods for studying the structures, energy levels and dynamics of chemical systems.[16] **Figure 1.14** displays the energy transitions associated with the many different portions of the electromagnetic spectrum.

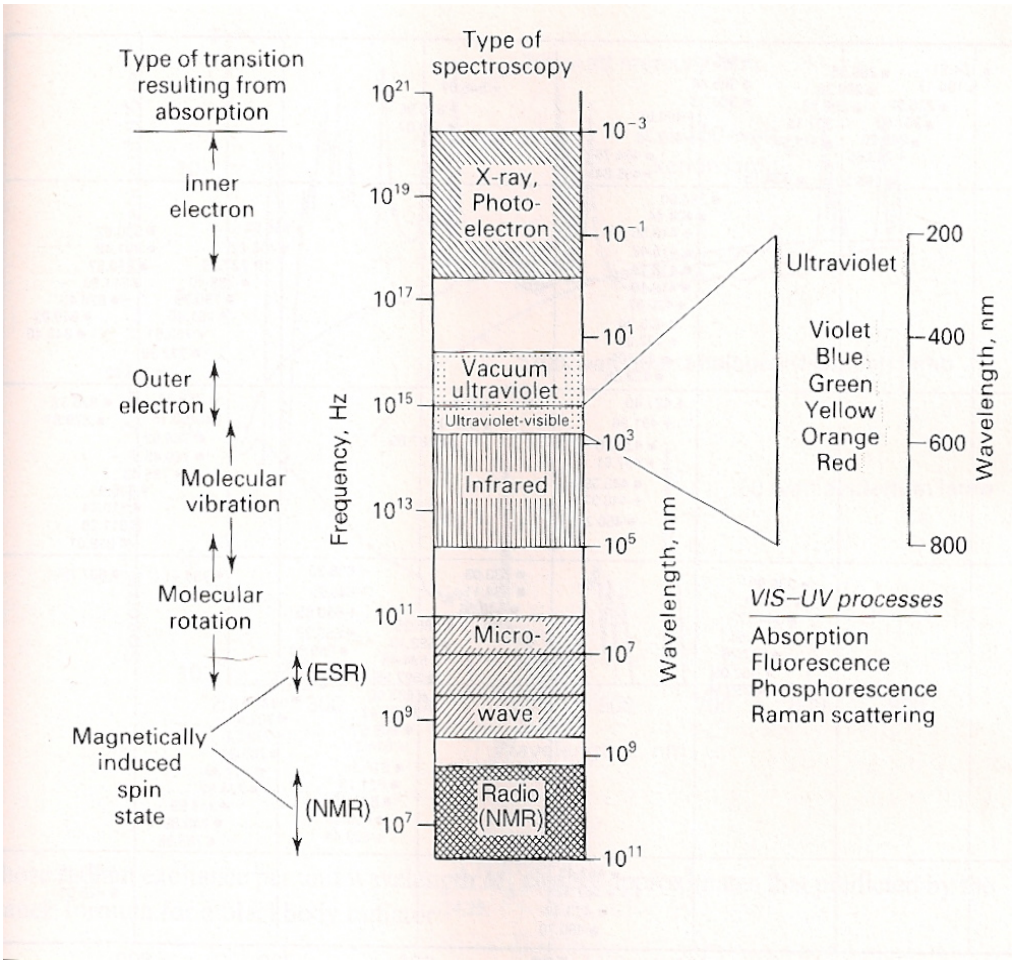


**Figure 1.14** The electromagnetic spectrum and its applications in spectroscopy[16]

It was 1800 when infrared radiations were first discovered by Frederic William Herschel,[36] and this field has proved to be a useful tool in the field of chemistry ever since. Infrared resonance (IR) spectroscopy is now one of the most powerful tools for quantitative and qualitative determination of molecules. Molecules have very specific frequencies at which they vibrate or rotate and which are characteristic to their energy levels. The infrared region of the electromagnetic spectrum, which is broken up into near-, mid-, and far infrared regions, extends from 10-10,000 $cm^{-1}$; however, the majority of molecular vibrations are contained in the mid infrared region from 400-4,000 $cm^{-1}$.

When the frequency of the radiation is the same as a vibrational frequency of the molecule, the molecule becomes excited and results in a loss of energy, which then yields an absorption band in the spectral data. When a molecule absorbs infrared radiation, the sample absorbs some of the radiation, but the rest will be transmitted. The intensity of the vibrations in the molecule increases as the infrared radiation absorbed increases. The frequency of the vibrations is represented by the relation

$$\upsilon = c/\lambda \qquad \text{Eq. (7)}$$

where c is the velocity of light and $\lambda$ is the wavelength.

Infrared resonance spectrosopy is a physical technique used in this investigation for characterization purposes.

# SECTION II:

# RESULTS AND CONCLUSION

## 2.1 Research Considerations

All chemicals were used as obtained without further purification. Cobalt(II) sulfate heptahydrate, tetrabutylammonium hydroxide and hydrofluoric acid (48-51%) were purchased from Aldrich. The ligand 5,5'-(1,4-phenylene)bis(1H-tetrazole) or 1,4-benzene, 5,5'-bistetrazole (**Figure 1.11**) was prepared according to methods found in literature [31,32,33] (further described in **1.4.8 1,4-Benzene Ditetrazole Synthesis**). All hydrothermal reactions were carried out in 23ml poly(tetrafluoroethylene)-lined stainless steel containers under autogenous pressure. Before heating, the reaction mixtures were stirred briefly and an initial pH was measured. The initial and final pH values were obtained using Hydrion pH measuring sticks. Water was distilled above 3.0 M Ω in-house using a Barnstead Model 525 Biopure Distilled Water Center.

## 2.2 Experimental Method

Porous coordination solids are prepared by combining solutions containing the appropriate organic ligands and metal ions at or near room temperature, and an attempt is made when designing their synthesis to exploit the directional nature of metal-ligand interactions for the construction of specific framework topologies.[20] The reaction parameters of this research

involves various additives, organic solvents or mixed aqueous solvents used and crystal growth rates as well as variations in temperature, pH, and stoichiometry in attempt to control the metal-ligand interactions for construction.

Each set of reaction conditions is reproduced three times, with each being subjected to 150, 180 and 200 °C. Each reaction vessel will contain either hydrogen fluoride or a strong base**,** which will effect the coordination of the medals to the tetrazole ligand. The addition of HF will help keep the reaction in solution. Each set of reactions will also be synthesized without an acid or base.

## 2.3 $[Co_2(H_{0.67}bdt)_3]\bullet 20H_2O$ ($H_2bdt$ = 1,4-benzene-5,5′-bistetrazole) Synthesis ($1\bullet 20H_2O$)

A solution of $CoSO_4\bullet 7H_2O$ (0.227g, 0.808mmol), 5,5'-(1,4-phenyllene)bis(1H-tetrazole) (0.100g, 0.467mmol), $H_2O$ (1,000g, 556mmol), and HF (0.100mL, 2.898mmol) in the mole ratio 1.73:1.00:1190:6.21 was heated at 180 °C for 48 hours. The initial and final pH was 2.2 and 2.0, respectively. Orange rods of $\mathbf{1}\bullet 20H_2O$ suitable for X-ray crystallography were isolated in 80% yield. An IR spectra (KBr pellet, $cm^{-1}$) was obtained and the peaks are as follows: 3404(br), 3077(w), 2889(w), 1693(m), 1558(m), 1437(s), 1273(m), 1236(w), 1191(w), 1162(m), 1069(s), 1003(m), 851(m), 768(w), 739(m), and 552(s).

Structural measurements were performed on a Bruker-AXS SMART-CCD diffractometer at 90 K using graphite-monochromated Mo-Kα radiation.

The data was corrected for Lorentz nd polarization effects and absorption using SADABS.[37,38] The structure was solved using direct methods. All calculations were performed using SHELXTL crystallographic software packages. The contribution of the solvent to the diffraction pattern in **1**•20$H_2O$ was eliminated from observable data using the SQUEEZE method implemented in PLATON. Crystal data for **1**•20$H_2O$: $C_3H_{6.5}Co_{0.25}N_3O_{2.5}$, orthorhombic, Cmmm, Mr = 139.34, a = 7.5320(6)A, c = 12.522(1)A, V = 2480.1(30)A $^{\Sigma}$, Z = 16, $\rho_{calc}$ = 1.493g $cm^{-1}$, $\mu$ = 0.762 $mm^{-1}$, F(000) = 1156, R1 = 0.0400, wR2 = 0.0901 (all data, 1781 reflections). The supplementary crystallographic data for this thesis can be obtained from the Cambridge Crystallographic Data Centre via www.cam.ac.uk/data_request/cif.

All low-pressure gas adsorption measurements were obtained using a Micromeritics ASAP 2020 volumetric gas adsorption instrument. The crystalline sample of **1**•20$H_2O$ was transferred to pre-weighted analysis tubes, which was then capped with a transeal. This prevents intrusion of atmospheric moisture during weighing and any transfer. The sample was evacuated under dynamic vacuum at 120 °C at a rate of 0.1 °C/min until the outgas rate was less than 2 mTorr/min.[40] The evacuated, capped tube containing the degassed **1**•20$H_2O$ was then weighed to determine the samples mass (100-175 mg).

For all isotherms, warm and cold free space correction measurements were taken using ultrahigh purity helium gas. The $H_2$ and $N_2$ isotherms at 77K were measured in liquid nitrogen baths using UHP grade gas sources. To

obtain the BET Nitrogen Adsorption Isotherm, the crystalline sample of $[Co_2(HBDT)_3]$•$20H_2O$ was evacuated under dynamic vacuum at 160°C and slowly dosed with $N_2$. To obtain the BET Hydrogen Adsorption Isotherm, the same procedure was applied, but was dosed with $H_2$, rather than $N_2$. The BET $H_2$ and BET $N_2$ sorption isotherms for **1**•$20H_2O$ were obtained at 77.4 K and are illustrated below in **Figure 2.1** and **Figure 2.2**, respectively.

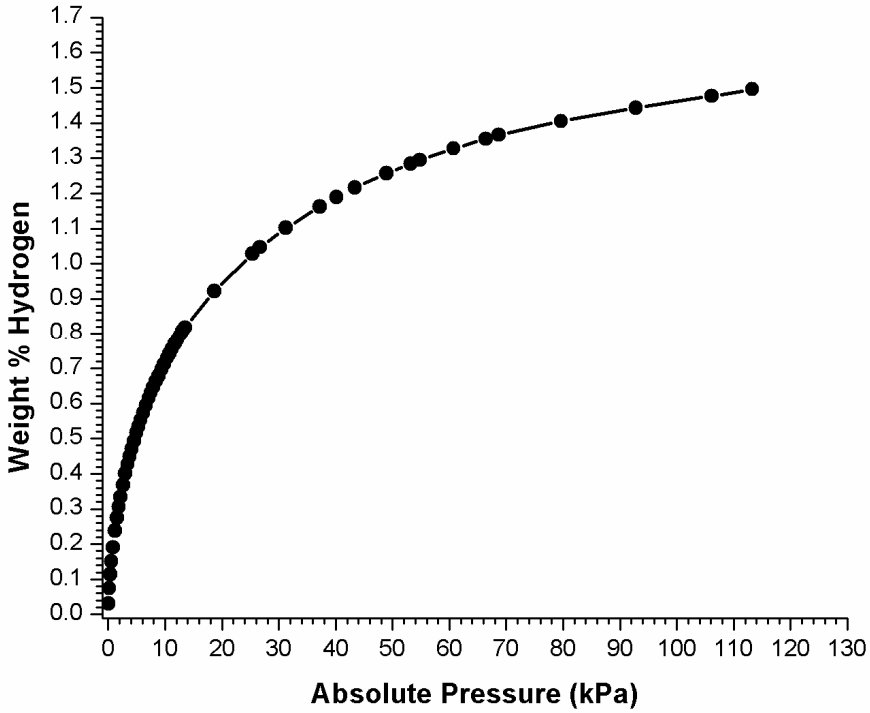


**Figure 2.1** BET $H_2$ Sorption Isotherm for 1•$20H_2O$ at 77.4 K

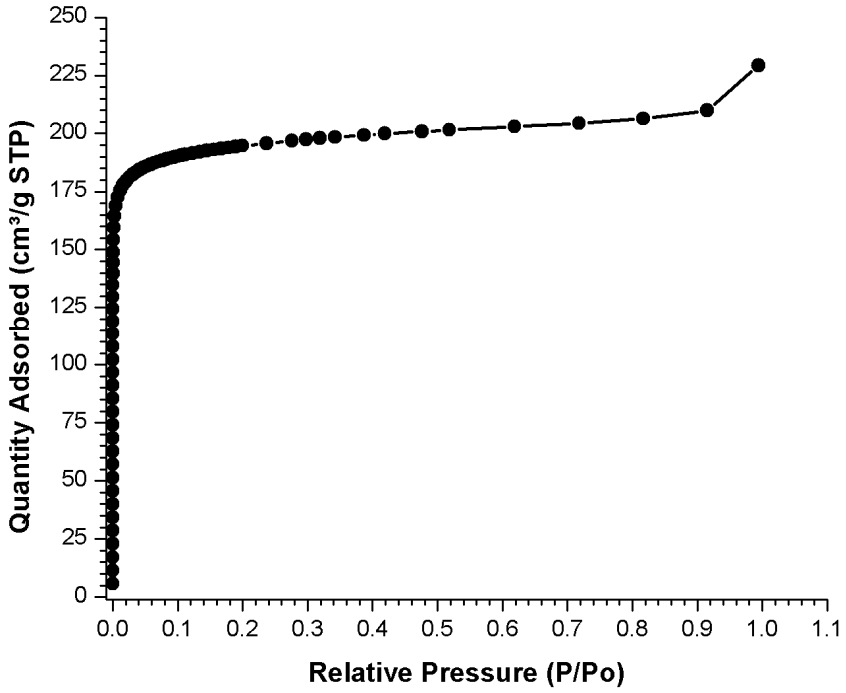


**Figure 2.2** BET $N_2$ Sorption Isotherm for 1•20$H_2O$ at 77.4 K

The BET surface area is 729 $m^2g^{-1}$, compared to a Langmuir surface area of 833 $m^2g^{-1}$, which corresponds to an accessible void volume of 47 % obtained via X-ray crystallography (PLATON). The Hydrogen Uptake Isotherm (**Figure 2.1**) demonstrated the material **1**•20$H_2O$ can absorb up to 1.495 % $H_2$ at 77K. This is impressive because few other compounds in literature illustrate this about of $H_2$ absorption under these conditions. The BET Nitrogen Adsorption plot (**Figure 2.2**) follows the BET theory (Eq. [1]). The $N_2$ Isotherm displays Type I Absorption demonstrating that **1**•20$H_2O$ is a microporous material. This was determined using the Adsorption isotherm IUPAC classifications illustrated in **Figure 1.1**.[25]

To obtain a Thermal Gravimetric Analysis (TGA), the crystalline sample of $[Co_2(HBDT)_3]$•$20H_2O$ was dosed with $N_2$ at 20mL/min and the temperature was raised from 25°C to 800°C at a rate of 5°C/min. The TGA profile (25-800 °C range) and Thermodiffractgram (25-425 °C range) for **1**•$20H_2O$ are illustrated below in **Figure 2.3** and **Figure 2.4**, respectively.

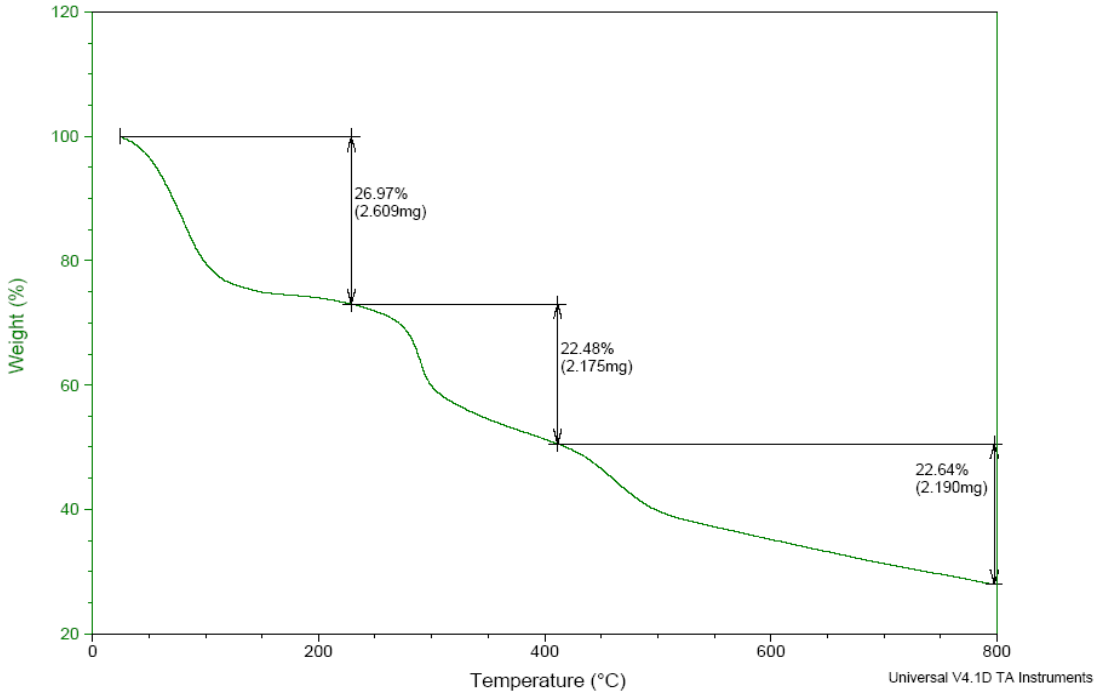


**Figure 2.3** TGA Profile of 1•$20H_2O$ in the 25-800 °C Range

The TGA revealed a 26.97 % weight loss (2.609 mg) between room temperature and 130°C attributed to the loss of water. There then was a plateau of stability from 130°C to 290°C, followed by decomposition of the ligand to 800 °C.

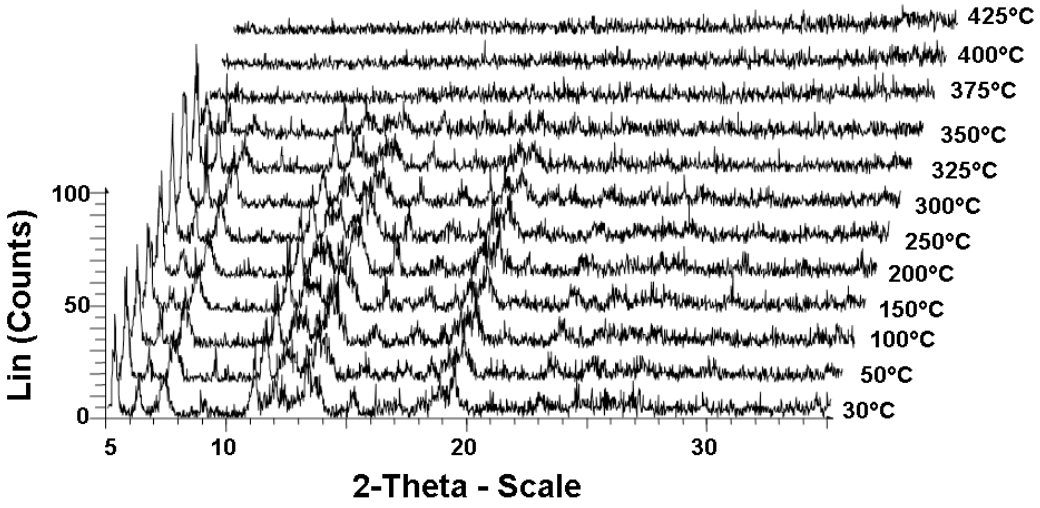


**Figure 2.4** Thermodiffractgram for 1•20$H_2O$ in the 25-425 °C Range

The thermodiffraction pattern in the 25-450$^oC$ range for **1**•20$H_2O$ is largely unchanged, indicating the compound's structural framework is thermally stable and is retained upon loss of water crystallization.

Computational data for [$Co_2$(HBDT)$_3$]•20$H_2O$ calculated by Density Functional Theory provided 47.1 % accessible void volume, and an availability of 774 $m^2$/g. The crystal system for this material is orthorhombic. The orthorhombic crystal system is a rectangular prism with a rectangular base (a by b) and height (c), where a, b, and c are all distinct which intersect at 90° angles.[41] In this material the unit cell dimensions of a, b, and c are 7.5320, 26.296 and 12.5221 Å respectively with a volume of 2480.1 Å. The

volume of the unit cell is 2480.1 Å, computed from the unit cell calculation of the dimensions a, b, and c. The empirical formula for the chosen unit cell is $C_3H_{5.75}\ Co_{0.38}N_3O_{2.13}$, with a formula weight of 139.95 g/mol. The density is calculated to be 1.499 $Mg/m^3$ from the crystal structure refinement data (**Appendix I**). Derived from the density and volume of a unit cell, the total mass of 1 unit cell is $3.7177 \times 10^{-7}$ mg.

Below, **Figure 2.5** and **Figure 2.6** are ball and stick representations of the $[Co_2(HBDT)_3]\bullet 20H_2O$ crystal structure.

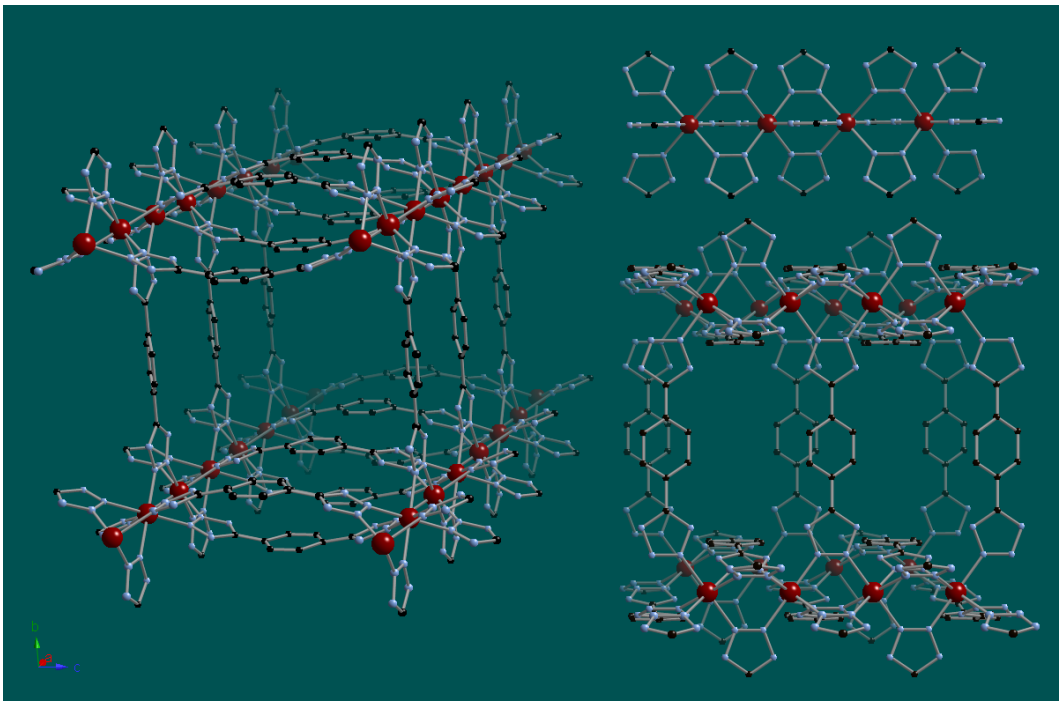

**Figure 2.5** Top Right: ball and stick representation of the $\{Co(tetrazolate)\}_n$ chain substructure of **1**•$20H_2O$. Left and bottom right: two views of the linking of chains through the phenyl tether of the BDT ligand

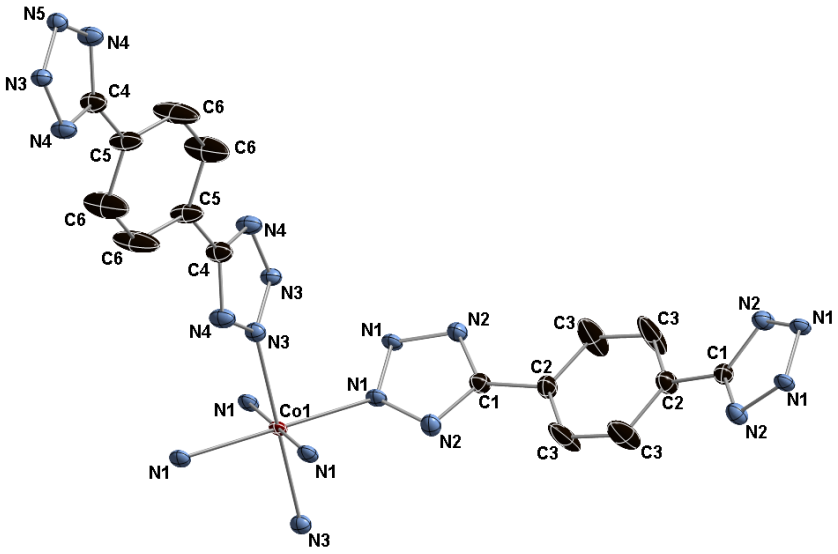


**Figure 2.6** Ball and stick representation of the structure of **1**•20$H_2O$ showing the atom-labeling scheme and 50% thermal ellipsoids

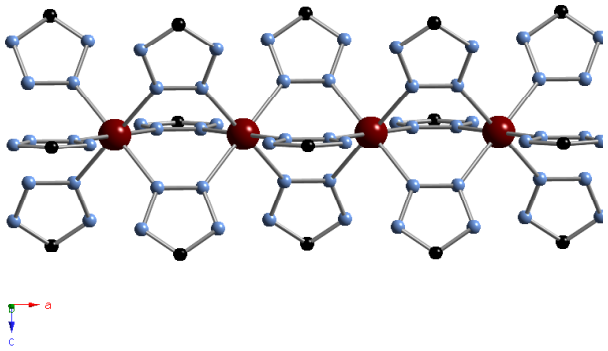

**Figure 2.7** Ball and stick representation of the cobalt-BDT chain

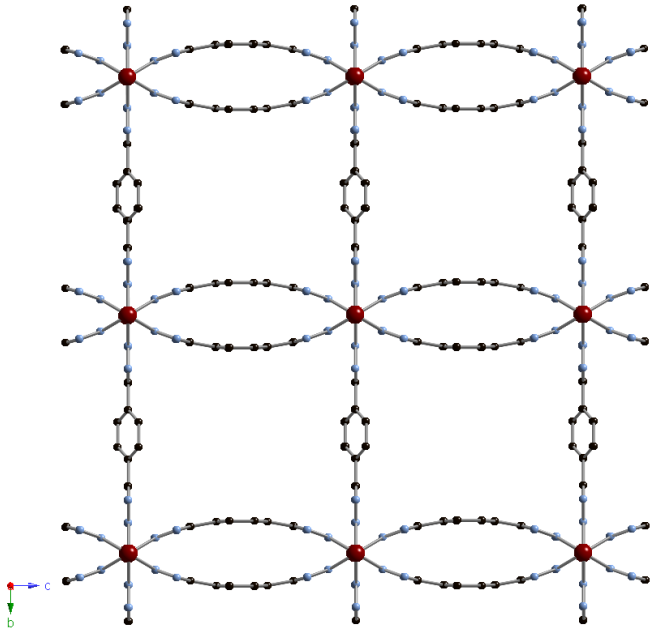

**Figure 2.8** Ball and stick representation of an additional view of **1**•20$H_2O$

The pore isosurface for **1**•20$H_2O$ calculated by Density Functional Theory provided there is a 47.1% accessible void volume (Planton) (**Figure 2.9**).

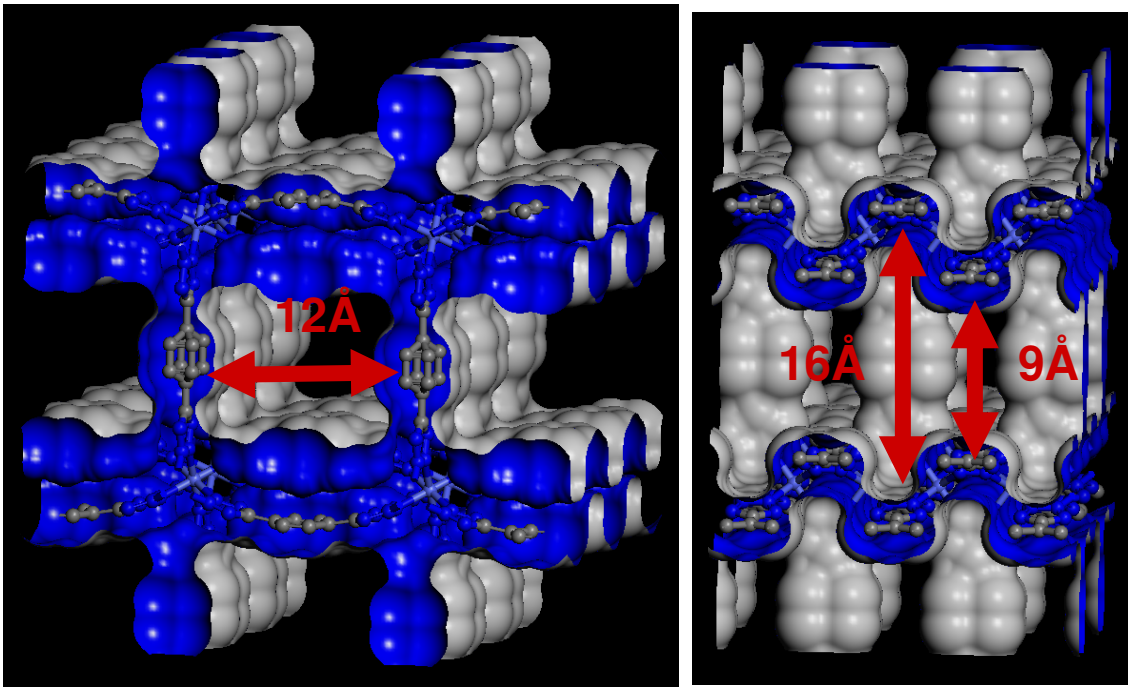


**Figure 2.9** Pore Isosurface

The connectivity pattern generates channels of approximate dimensions 16.0 Å x 12.0 Å x 9.0 Å, corresponding to 47.1% of the unit cell volume, which are occupied by water molecules of crystallizaion.

## 2.4 $(Me_2NH_2)[Cu_4Cl(tba)_4(H_2O)_4]\bullet 15H_2O$ Synthesis

A solution of $CuCl_2$ (0.200g, 1.487mmol), 4-(1H-tetrazol-5-yl)-benzoic acid ($H_2$tba) (0.050g, 0.3378mmol), $H_2O$ (100g, 55.6mmol), dimethylforamide (4.72g, 64.60mmol), methanol (3.959g, 123.56mmol) in the mole ratio 4.40:1.00:164.59:191.24:365.78 was reacted, while stirring with 2 drops hydrochloric acid for 5 minutes. Blue rods of **2**•15$H_2O$ suitable for X-ray crystallography were visible after 7 days at room temperature. These crystals were isolated for X-Ray crystallography.

Structural measurements were performed on a Bruker-AXS SMART-CCD diffractometer at 90 K using graphite-monochromated Mo-Kα radiation. The data was corrected for Lorentz nd polarization effects and absorption using SADABS.[37,38] The structure was solved using direct methods. All calculations were performed using SHELXTL crystallographic software packages. The contribution of the solvent to the diffraction pattern in **2**•15$H_2O$ was eliminated from observable data using the SQUEEZE method implemented in PLATON.

All low-pressure gas adsorption measurements were obtained using a Micromeritics ASAP 2020 volumetric gas adsorption instrument. The crystalline sample of **2**•15$H_2O$ was transferred to pre-weighted analysis tubes,

which was then capped with a transeal. This prevents intrusion of atmospheric moisture during weighing and any transfer. The sample was evacuated under dynamic vacuum at 120 °C at a rate of 0.1 °C/min until the outgas rate was less than 2 mTorr/min.[40] The evacuated, capped tube containing the degassed **2**•15$H_2O$ was then weighed to determine the sample's mass.

For all isotherms, warm and cold free space correction measurements were taken using ultrahigh purity helium gas. The $H_2$ and $N_2$ isotherms at 77K were measured in liquid nitrogen baths using UHP grade gas sources. To obtain the BET Nitrogen Adsorption Isotherm, the crystalline sample of **2**•15$H_2O$ was evacuated under dynamic vacuum at 160$^{o}$C and slowly dosed with $N_2$. To obtain the BET Hydrogen Adsorption Isotherm, the same procedure was applied, but was dosed with $H_2$, rather than $N_2$. The BET $H_2$ and BET $N_2$ sorption isotherms for **2**•15$H_2O$ were obtained at 77.4 K and are illustrated below in **Figure 2.10** and **Figure 2.11**, respectively.

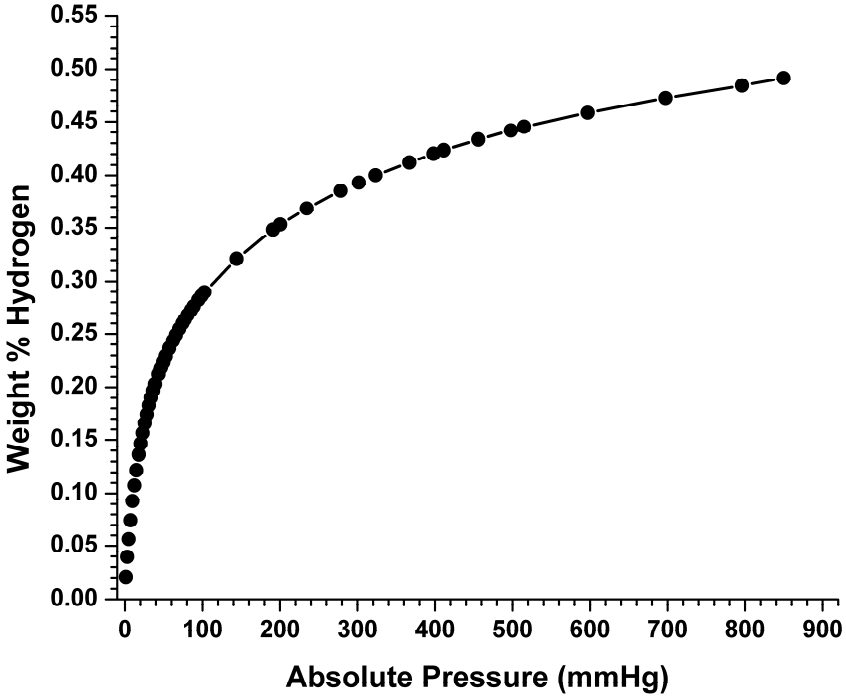


**Figure 2.10** BET $H_2$ Sorption Isotherm for **2**•$15H_2O$ at 77.4 K.

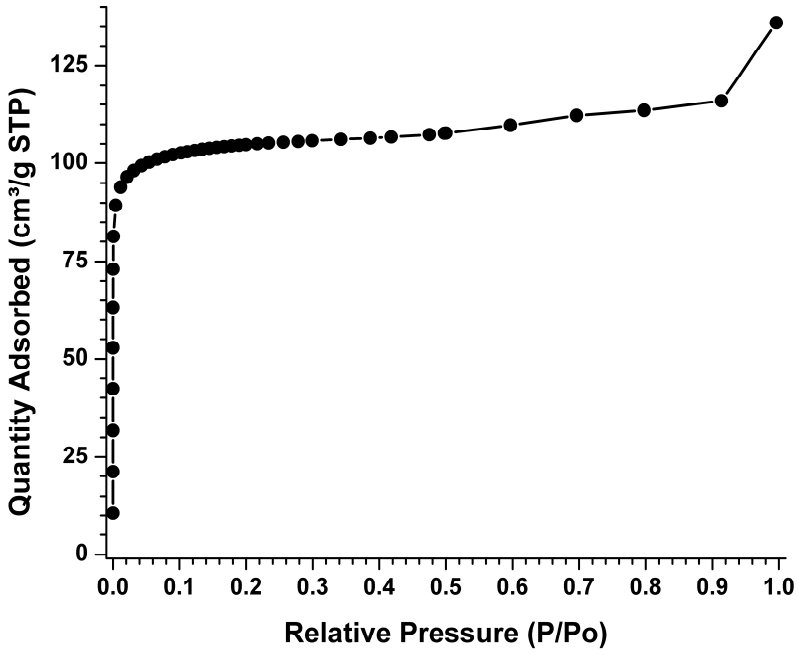


**Figure 2.11** BET $N_2$ Sorption Isotherm for **2**•$15H_2O$ at 77.4 K.

The BET Nitrogen Adsorption plot (**Figure 2.11**) follows the BET theory (Eq. [1]). The $N_2$ Isotherm displays Type I Absorption demonstrating that **2**•15$H_2O$ is a microporous material. This was determined using the Adsorption isotherm IUPAC classifications illustrated in Figure **1.1**.[25]

To obtain a TGA, the crystalline sample of **2**•15$H_2O$ was dosed with N2 at 20mL/min and the temperature was raised from 25°C to 800°C at a rate of 5°C/min. The TGA profile for **2**•15$H_2O$ is illustrates below in **Figure 2.12**.

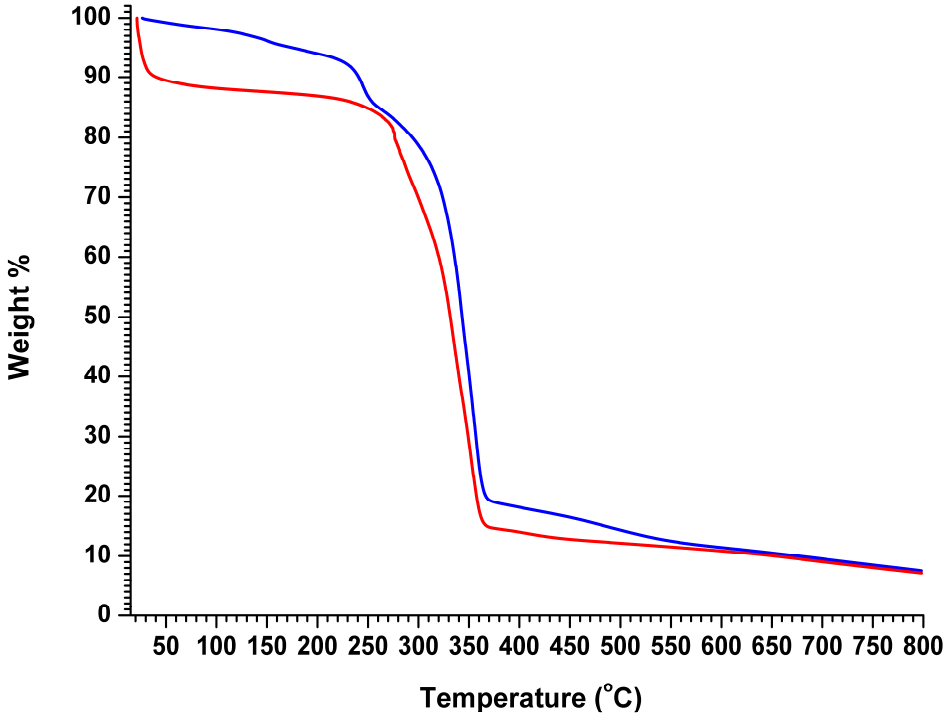


**Figure 2.12** TGA Profile of **2**•15$H_2O$ in the 25-800 °C Temperature Range

The framework of **2**• 15$H_2O$ (**Figure 2.13**) is constructed from $\{Cu_4(\mu_4\text{-}Cl)(H_2O)_4\}^{7+}$ clusters (**Figure 2.14**) linked through the $tba^{2-}$ ligands (**Figure 1.11**).

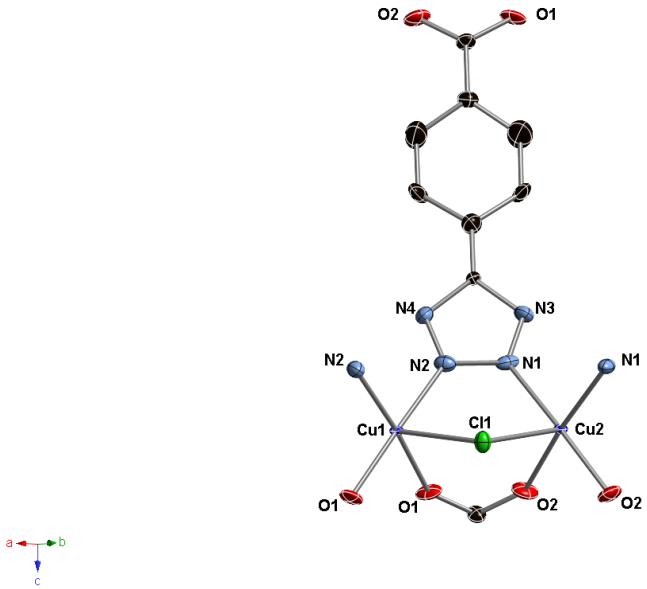


**Figure 2.13** Ball and stick representation of the structure of **2** •15$H_2O$ showing the atom-labeling scheme.

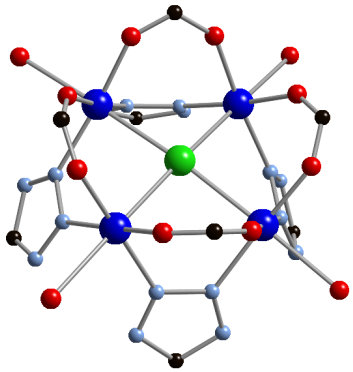

**Figure 2.14** $\{Cu_4(\mu_4\text{-}Cl)(H_2O)_4\}^{7+}$ clusters used in the framework of **2**•15$H_2O$

Additional views of the 3-D structure of 2•15$H_2O$ are illustrated below in **Figure 2.15** and **Figure 2.16**.

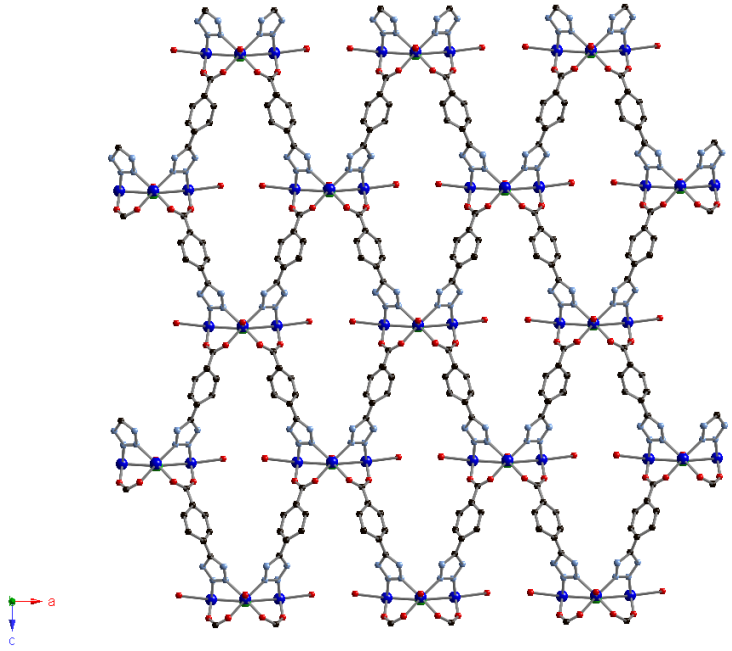

**Figure 2.15** Additional view of **2**•15$H_2O$

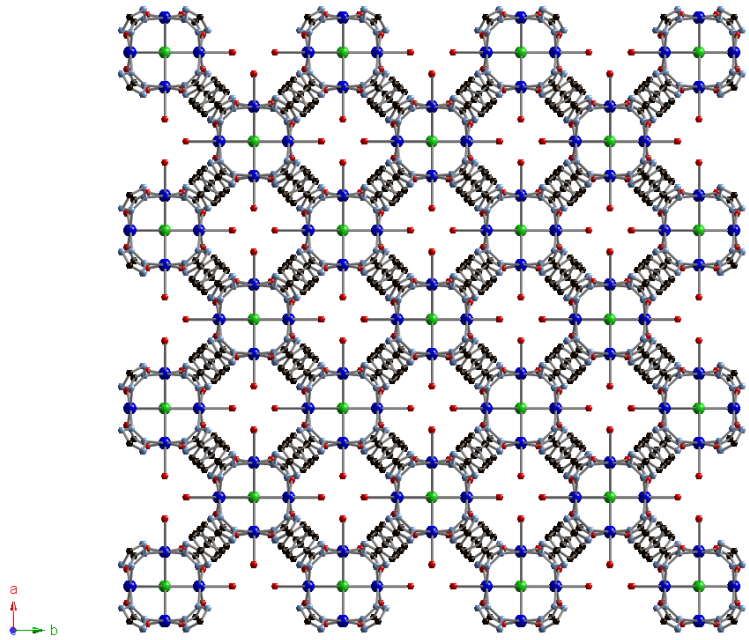

**Figure 2.16** Additional view of **2**•15$H_2O$

The aqua ligands project into the void domain of the structure, which is also occupied by the $(CH_3)_2NH_2^+$ cations.

The pore isosurface for **2**•15$H_2O$ calculated by Density Functional Theory provided there is a 65.0% accessible void volume (PLATON) (**Figure 2.17**).

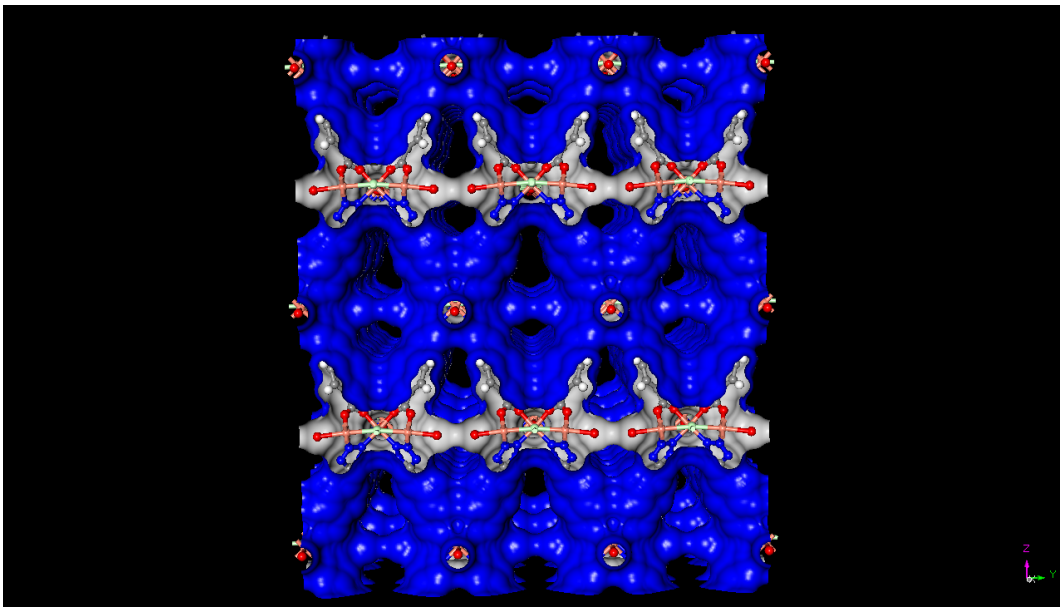

**Figure 2.17** Pore Isosurface of **2**•15$H_2O$

# SECTION III:

# CONCLUSION

## 3.1 Conclusion

The research in this investigation involves the synthesis and characterization of hybrid inorganic/organic frameworks using various metals and organic ligands. Varying reaction conditions, ligand tether length and solvents allowed the examination of these frameworks' structural versatility. In addition, physical properties were examined to determine characteristics such as gas adsorption and stability.

## 3.1 $[Co_2(H_{0.67}bdt)_3]\bullet 20H_2O$ ($H_2bdt$ = 1,4-benzene-5,5′-bistetrazole)

In an attempt to synthesize a framework with the greatest gas uptake capabilities, the ligand 1,4-benzene-5,5′-bistetrazole (1,4-BDT) was reacted with $CoSO_4$ under various conditions. These include the addition of a base, the addition of an acid, varying the temperature and the amount of time in specific temperatures. The framework $[Co_2(H_{0.67}bdt)_3]\bullet 20H_2O$ has an accessible void volume of 47.0% obtained via X-ray crystallography. The Hydrogen Uptake Isotherm (**Figure 2.1**) demonstrated the material $[Co_2(H_{0.67}bdt)_3]\bullet 20H_2O$ can absorb up to 1.495 % $H_2$ at 77K, which is an impressive physical property because few other compounds in literature illustrate this about $H_2$ absorption under these conditions.

## 3.2 $(Me_2NH_2)[Cu_4Cl(tba)_4(H_2O)_4]\bullet 15H_2O$

The framework of $(Me_2NH_2)[Cu_4Cl(tba)_4(H_2O)_4]\bullet 15H_2O$ is constructed from $\{Cu_4(\mu_4\text{-}Cl)(H_2O)_4\}^{7+}$ clusters (**Figure 2.14**) linked through the $tba^{2-}$ ligands. This structure is an additional attempt to synthesize a framework with the greatest hydrogen storage capabilities by varying temperature and solvents. To obtain this framework, no attempt was made to add a base, only acid; however, the type of acid was varied. The pore isosurface for $(Me_2NH_2)[Cu_4Cl(tba)_4(H_2O)_4]\bullet 15H_2O$ calculates by Density Functional Theory provided there is a 65.0% accessible void volume as opposed to 47.0% for the $[Co_2(H_{0.67}bdt)_3]\bullet 20H_2O$ framework.

**SECTION IV:**

**SOURCES CITED AND APPENDICES**

## 4.1 Sources Cited

[1] Atkins, P.; Overton, T.; Rourke, J.; Weller, M.; Armstrong, F. *Inorganic Chemistry*. Oxford University Press, New York: **2006**.

[2] Ouellette, W.; Prosvirin, A. V.; Whitenack, K.; Dunbar, K. R.; Zubieta, J. *Angew. Chem. Int. Ed.* **2009**, 48, 2140-2143.

[3] Ouellette, W.; Prosvirin, A.V.; Chieffo, V.; Dunbar, K.R.; Hudson, B.; Zubieta, J., *Inorg. Chem*. **2006**, 45, 9346-9366.

[4] Eitzen D., Stanley; Zinn, Maxine Baca. *Social Problems*. Pearson Education, Inc., New York: **2006**.

[5] Rh Value Publishing. 1987. "Complete History of the Ford Motor Company." Crescent: 1987

[6] Kay, Jane Holtz. 2004. "Our Culture's Excess Rolls toward Oblivion." *Los Angeles Times* (May 31). Online. Available: http://www.latimes.com/news/opinion/commentary/la-oe-kay3/may31.

[7] Hoagland, Jim. 1997. "Crisis Management in a Fog." *National Post Weekly Edition* (December 1): 5-6.

[8] Ouellette, W. *Structural Diversity of the Oxovanadium Organodiphosphonate and the M(I,II)/1,2,4-trizolate Systems: A Platform for the Design of Multifunctional Hybrid Orgaic-Inorganic Materials.* **2007**.

[9] "Hydrogen Posture Plan", United States Department of Energy, February **2004**. http://www.eere.energy.gov/hydrogenandfuelcells/pdfs/hydrogen_posture_plan.pdf.

[10] "Basic Research Needs for the Hydrogen Economy", United States Department of Energy, report of the Basic Energy Sciences Workshop on Hydrogen Production, Storage, and Use, May 13-15, **2003**.

[11] King, K. S. W.; Everette, D. H.; Haul, R. A. W.; Moscou, L.; Pierotte, R. A.; Rouquerol, J.' Siemieniewska, T. *Pure Appl. Chem.* **1985**, 57, 603.

[12] International Union of Pure and Applied Chemistry (**1994**). "van der Waals forces". *Compendium of Chemical Terminology* Internet edition.

[13] Gregg, S. J.; Sing, K. S. W. *Adsorption, Surface Area and Porosity*, 2nd ed.; Academic: London, **1982**.

[14] T. J. Barton, L. M. Bull, W. G. Klemperer, D. A. Loy, B. McEnaney, M. Misono, P. A. Monson, G. Pez, G. W. Scherer, J. C. Vartuli, and O. M. Yahgi, *Chem. Mater.* **1999**, 11, 2633-2656.

[15] Ruthven, D. M. *Principles of Adsorption and Adsorption Processes*; John Wiley: New York, **1984**.

[16] Garland, Carl W.; Nibler, Joseph W.; Shoemaker, David P. *Experiments in Physical Chemistry*. McGraw-Hill Higher Education, New York: **2003**.

[17] Aaron Nackos Power Point. Adsorption, Surface Area, and Porosity.

[18] Laidler, Keith J.; Meiser, John H.; Sanctuary, Bryan C. *Physical Chemistry*. Houghton Mifflin Company, New York: **2003**.

[19] Langmuir, I. *J. Am. Chem. Soc.* **1913**, *35*, 931; **1915**, *37*, 1139; **1918**, *40*, 1361.

[20] Barton, T. J.; Bull, L. M.; Klemperer, W. G.; Loy, D. A.; McEnaney, B.; Misono, M.; Monson, P. A.; Pez, G.; Scherer, G. W.; Vartuli, J. C.; Yaghi, O. M. *Chem. Mater.* **1999**, *11*, 2633-2656.

[21] Atkins, Peter; Paula, Julio de. *Physical Chemistry*. W.H. Freeman and Company, New York: **2006**.

[22] Silva, N. J. O.; Amaral, V. S.; Carlos, L. D.; de Zea Bermudez, V., *J. Appl. Phys.* **2003**, 93, 6978-6980.

[23] Kahn, O. *Molecular Magnetism*; VCH: New York, **1993**.

[24] Forster, P.M.; Cheetham, A.K., *Top. Caral.* **2003**, 24, 79-86.

[25] Hagrman, P.J.; Hagrman, D.; Zubieta, J., *Angew. Chem. Int. Ed.* **1999**, 38, 2638-2684.

[26] Houghton, R. P.; Elmore, D. T.; Lewis, J.; Schofield, K.; Thomas, J. M. *Metal Complexes in Organic Chemistry*. Cambridge University Press, New York: **1979**.

[27] Carey, Francis A. *Organic Chemistry*. McGraw-Hill Higher Education, New York: **2006**.

[28] R. Patel, M. T. Weller, D. J. Price, *Dalton Trans*. **2007**, 4034-4039.

[29] Ouellette, W.; Prosvirin, A. V.; Valeich, J.; Dunbar, K. R.; Zubieta, J. *Inorg. Chem.* **2007**, 46, 9067-9082.

[30] Submitted for Publication: April 2009.

[31] Cui, Y.; Ngo, H.L.; Lin, W. *Inorg. Chem.* **2002**, 41, 5940-5942.

[32] Zanon, J.; Klapars, A; Buchwald, S.L. *Am. Chem. Soc.* **2003**, 125, 2890-2891.

[33] Mircea, D.; Dailly, A.; Liu, L.; Brown, C.M.; Neumann, D.A.; Long, J.R. *J. Am. Chem. Soc.* **2006**, 128, 16876-16883.

[34] Batsanov, A. S.; Howard, J. A. K. *Diffraction Methods in Inorganic Chemistry*. John Wiley & Sons, Ltd., New York, NY: **2006**.

[35] Whiston, C. *X-Ray Methods*. John Wiley & Sons, Ltd., New York, NY: **1987**.

[36] Avram, M.; Mateescu, G. H. *Infrared Spectroscopy, Applications in Organic Chemistry*. Wiley- Interscience, New York, NY: **1966**.

[37] SAINT *Plus, Date Reduction Software*, version 6.45A; Bruker AXS Inc.: Madison, WI, **1997-2002**.

[38] Sheldrick, G. M. SADABS; University of Gottingen: Gottingen, Germany, **1996**.

[39] D.J. Collins, H.-C. Zhou, *J. Mater. Chem.* **2007**, 17, 3154-3160.

[40] Ouellette, W.; Prosvirin, A.V.; Valeich, J.; Dunbar, K. R.; Zubieta, *J. Inorg. Chem.* **2007**, 46, 9067-9082.

[41] Hurlbut, Cornelius S.; Klein, Cornelis, **1985**, *Manual of Mineralogy*, 20th ed., pp. 69 – 73.

[42] Haasnoot, J. G. *Coord. Chem. Rev*. **2000**, 200-202, 131-185.

## 4.2 Appendix I

Crystal data and structure refinement for $[Co_2(Trz)_3]\bullet 20H_2O$

| | | |
|---|---|---|
| Identification code | cmmm | |
| Empirical formula | C3 H5.75 Co0.38 N3 O2.13 | |
| Formula weight | 139.95 | |
| Temperature | 98(2) K | |
| Wavelength | 0.71073 Å | |
| Crystal system | Orthorhombic | |
| Space group | Cmmm | |
| Unit cell dimensions | a = 7.5320(6) Å | a= 90°. |
| | b = 26.296(2) Å | b= 90°. |
| | c = 12.5221(10) Å | g = 90°. |
| Volume | 2480.1(3) $Å^3$ | |
| Z | 16 | |
| Density (calculated) | 1.499 $Mg/m^3$ | |
| Absorption coefficient | 1.077 $mm^{-1}$ | |
| F(000) | 1150 | |
| Crystal size | 0.22 x 0.14 x 0.12 $mm^3$ | |
| Theta range for data collection | 1.55 to 28.07°. | |
| Index ranges | -9<=h<=9, -34<=k<=34, -16<=l<=16 | |
| Reflections collected | 13038 | |
| Independent reflections | 1728 [R(int) = 0.0411] | |
| Completeness to theta = 28.07° | 100.0 % | |
| Absorption correction | None | |
| Refinement method | Full-matrix least-squares on $F^2$ | |
| Data / restraints / parameters | 1728 / 0 / 81 | |
| Goodness-of-fit on $F^2$ | 1.089 | |
| Final R indices [I>2sigma(I)] | R1 = 0.0355, wR2 = 0.0881 | |
| R indices (all data) | R1 = 0.0400, wR2 = 0.0901 | |
| Largest diff. peak and hole | 0.595 and -0.349 $e.Å^{-3}$ | |